Volume 1 | Number 1 | Jan 2013 | Pages 1–100

Journal of
Materials Chemistry A

Materials for energy and sustainability
www.rsc.org/materialsA

ROYAL SOCIETY
OF CHEMISTRY

ROYAL SOCIETY
OF CHEMISTRY

www.rsc.org/materialsA

Journal of Materials Chemistry A

ARTICLE

Selective adsorption of contaminants on Pb(Zr,Ti)O$_3$ surfaces evidenced by X-ray photoelectron spectroscopy

Laura Elena Ştoflea,[a] **Nicoleta Georgiana Apostol,**[a] **Lucian Trupină,**[a] **and Cristian Mihail Teodorescu*[a]**

X-ray photoelectron spectroscopy (XPS) analyses on lead zirco-titanate Pb(Zr,Ti)O$_3$(001) single crystal thin layers as function on the time spent between sample preparation by pulsed laser deposition and introduction in ultrahigh vacuum revealed the fact that freshly prepared samples showed a shift of the C 1s towards higher binding energy, together with shifts of core levels originating from the substrate 10 (particularly Ti 2p and O 1s) towards lower binding energy. This behaviour is explained by considering that the molecules of contaminants (fatty acids, alcohols, esters) are adsorbed preferentially on areas exhibiting outwards polarization $P^{(+)}$. Thus, photoelectrons originating from contaminants will experience larger binding energies owing to the charge state of the $P^{(+)}$ areas, whereas the substrate XPS signals from these $P^{(+)}$ areas are attenuated by the contaminants, with the consequence of prevalence of XPS substrate 15 signals originating from $P^{(-)}$ areas, shifted towards lower binding energies. Piezoresponse force microscopy confirmed the assumptions derived by XPS and suggest the existence of an interplay between the adsorption of contaminants and the surface polarization state.

Introduction

Ferroelectric single crystal surfaces are a hot topic nowadays, 20 justified by the tremendous number of applications of these materials in ferroelectric memories[1], piezoelectric and pyroelectric devices[2]. To these functionalities, controlled adsorption of molecules onto ferroelectrics might be important in heterogenous catalysis, where such adsorption processes are 25 essential[3].

Several examples of such applications were recently reported, by using temperature programmed-desorption (TPD) [4-7]. Differences of 100 K are observed between the desorption temperatures of polar molecules (2-propanol[4] or acetic acid[5]), 30 from LiNbO$_3$(0001) exhibiting outwards $(P^{(+)})$ or inwards $(P^{(-)})$ polarization. For non-polar molecules (dodecane[5]) no dependence on the initial polarization state of the substrate is reported. Dissociative adsorption on polar surfaces (e.g. 2-fluoroethanol) may occur, with differences in the activation energies of product 35 formation (acetaldehyde) between different substrate (BaTiO$_3$) polarization state[6]. Similar results (15-20 K desorption temperature differences) are reported on water and methanol on LiNbO$_3$[7].

There is also an interplay between surface chemical reactions 40 and the ferroelectric polarization state. Recently, it was shown that oxygen adsorption at the surface of PbTiO$_3$ is able to reverse its polarization[8]. Water is dissociatively adsorbed, with -OH radicals bonded to Ti^{4+} surface ions, modifying the surface rumpling of the ferroelectric layer[9]. Therefore, chemical reactions 45 at ferroelectric surfaces may be thought as an emerging field in

technology[10].

During the last years, one may notice an increasing interest in ferroelectric surfaces as model catalysts[11,12]. The basic phenomena stimulating the interest in ferroelectrics catalysis 50 relies on the ability of charge separation inside a film presenting out-of-plane polarization, since the internal (depolarization) field transports electrons towards the $P^{(+)}$ oriented face and holes at the opposite face. Therefore, the $P^{(+)}$ face will be active for reduction, and the $P^{(-)}$ face will be active for oxidation[11]. Recently, a direct 55 *in situ* determination of the polarization dependence of physisorption on ferroelectric surfaces by TPD revealed noticeable differences in the energetics of physisorption on ferroelectric domains with different polarization for CH$_3$OH and CO$_2$ on BaTiO$_3$ and Pb(Ti$_{0.52}$Zr$_{0.48}$)O$_3$ surfaces[12]. Also, efficient 60 water photolysis (oxidation to O$_2$) was reported recently on BiFeO$_3$ layers prepared by chemical vapor deposition exhibiting ferroelectric and ferromagnetic properties[13] and one can infer that the high activity of these layers is mainly connected to their ferroelectric properties. It starts nowadays to be acknowledged 65 that ferroelectric polarization improves surface reaction rates of gaseous species, therefore ferroelectric catalysts might be envisaged as alternatives to high-cost precious metals.

A certified method for nondestructive analysis of the surface ferroelectric state is X-ray photoelectron spectroscopy (XPS)[14-17]. 70 The band bending at ferroelectric surfaces exhibiting out-of-plane polarization is expressed, in terms of binding energies (BE) as $\Delta\Phi = eP\delta/\varepsilon$ (Fig. 1), where e is the elementary charge, P is the out-of-plane polarization (positive when oriented outwards), ε is

the permittivity of the layer, and δ the distance between the surface and the depth where the mobile carriers accumulate owing to the depolarization field (Fig. 1)[18,19]. For $PbZr_{0.2}Ti_{0.8}O_3$ (PZT 20/80), with a strong value of the polarization ($\sim$ 1 C/m^2)[20], values close to 1 eV are reported for $\Delta\Phi$ [15-17].
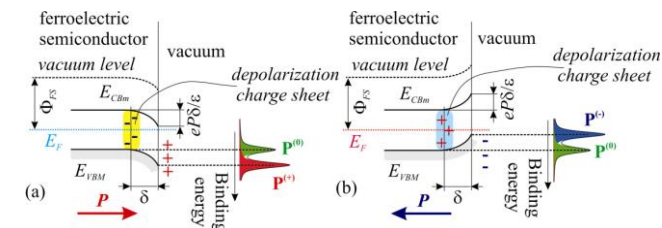
Fig. 1. Band diagrams at free ferroelectric surfaces: (a) outwards polarization; (b) inwards polarization.

The fact that core levels are rigidly shifted with the band bending has been demonstrated[16] for PZT. Therefore, XPS allows one to directly derive the relative proportion of areas with outwards $P^{(+)}$, inwards $P^{(-)}$, or no polarization perpendicular to the surface $P^{(0)}$. However, more complicated problems might occur, mostly related to the surface charging during the photoemission process (see the Experimental section). Quite often, the C 1s level from the inherent contamination on samples introduced from ambient atmosphere is used as a calibration, by setting the C 1s level to 284.6 eV[21]. This C 1s is related to hydrocarbons C-C-..., bonds, but oxygen should also be present in these molecules to ensure creation of molecular dipoles and sticking on surfaces[22]. This paper will demonstrate also that sometimes this re-calibration procedure is inaccurate.

Experimental

Sample preparation

Single crystal 150 nm thick PZT layers are grown by pulsed laser deposition (PLD) on $SrTiO_3$ with a $SrRuO_3$ (20 nm) buffer layer as bottom electrode. The PLD setup (Surface) operated with KrF radiation (248 nm wavelength), 0.7 J x 20 ns pulses, repetition rate 5 Hz, laser fluence 2 J/cm^2. During the growth, the substrate was heated at 575 °C in partial O_2 pressure of 0.2 mbar[15-18]. Samples were regularly checked by reflection high energy electron diffraction, X-ray diffraction[15], atomic force microscopy (AFM), piezoresponse force microscopy (PFM) and high resolution transmission electron microscopy[15,18]. These investigations evidenced a good epitaxial quality of the films. All samples discussed in this paper are produced during the same PLD run. After preparation by PLD, samples experienced ambient atmosphere before being introduced in the photoemission setup. After preparation and cooling down in oxygen atmosphere, the samples were extracted from the PLD machine and stored in clean, hermetic plastic boxes, without any physical contact to their surface. There is no organic chemistry lab close to neither the PLD or the XPS labs.

Sample characterization

XPS measurements were performed in a photoemission setup (Specs) operating in ultrahigh vacuum (UHV) in a base pressure of low 10^{-10} mbar vacuum range. Monochromatic Al K$_{\alpha 1}$ radiation (1486.74 eV) was used, and the pass energy of the analyzer was set to 30 eV. The total full width at half maximum obtained in these conditions on single crystal surfaces is around 0.9 eV[23,24]. Charging effects are eliminated by adjusting the X-ray power (400 W) and the electron flood gun (1 eV/ 0.1 mA). Annealing of the sample was performed in 10^{-9} mbar pressure range. AFM and PFM images were taken at ambient atmosphere using an Asylum Research setup on twin samples produced in the same run. PFM writing of areas of well defined polarization is achieved by applying on a conductive tip voltages of + 10 V for $P^{(-)}$ areas (inwards polarization) or - 10 V for $P^{(+)}$ areas (outwards polarization).

Results and discussions

Photoemission data

In the following, we will concentrate on three PZT samples: (i) the 'fresh' sample, introduced in the XPS setup immediately (15 min.) after its preparation by PLD; (ii) the '1 week old' sample, produced in the same PLD run, but introduced inside the UHV chamber one week after the preparation, and (iii) the 'annealed' sample (in ultrahigh vacuum, UHV). Annealing produces a surface with a majority of $P^{(+)}$ polarization[16,17,20]. Samples which are not annealed may present domains with $P^{(+)}$ and $P^{(-)}$ polarizations[15,18]. Between the preparation and the XPS measurements the samples are stored in clean boxes, in ambient atmosphere.

Figure 2 presents the photoemission data. We remark a demonstration of the rigid shift of the Pb 5d$_{3/2}$ core level with the valence band offset (Fig. 2(a)). The electron distribution curves (EDCs) from Figs. 2(b-f) are analyzed with Voigt lines plus Voigt integrals to simulate inelastic backgrounds[15-18,26]. C 1s and O 1s are fitted with singlets, whereas Ti 2p, Zr 3d and Pb 4f are fitted with doublets with fixed branching ratios to their theoretical values (2 for 2p, 1.5 for 3d, 1.333... for 4f). The Gauss width was the same for all components, the Lorentz width is allowed to vary for Ti 2p only, to account for Coster-Kronig decay channels of the 2p$_{1/2}$ core state[27]. The Lorentz width does not vary for Zr 3d and Pb 4f spectra, since the corresponding spin-orbit splitting (2.38 and 4.86 eV) is lower than the estimated ionization energy of PZT $E_i = \Phi + (E_F - E_{VBM})$, see Fig. 1 and note that $\Phi = 5.1 - 5.4$ eV[15-18]. Therefore, Coster-Kronig decay channels consisting in ejection of a valence electron following a filling of a 2p$_{1/2}$ vacancy by a 2p$_{3/2}$ electron cannot manifest in these cases.

From this analysis, the surface sample composition may be derived as $PbZr_{0.4}Ti_{0.6}O_{2.5}$ + 0.5 PbO + 0.14 Pb(CO$_3$)$_2$ + (contaminants) for the 'fresh' sample, $PbZr_{0.35}Ti_{0.65}O_{2.6}$ + 0.12 Pb(CO$_3$)$_2$ + (contaminants) for the '1 week old' sample and $PbZr_{0.2}Ti_{0.8}O_{2.4}$ + 0.12 PbCO$_3$ + (contaminants) for the 'annealed' sample. Note the slightly different Ti/Zr ratio obtained at the surface, although all samples were prepared in the same run. For deriving the PZT composition, the total (Zr + Ti) intensities are taken into account, with the lowest BE components of O 1s and Pb 4f. The second BE components of Pb 4f (139.41 eV, 138.81 eV and 139.06 eV) and O 1s (529.51 eV, 531.02 eV and 530.65 eV) are mixed in the carbonate compound, together with the C 1s lines at (290.23 eV, 289.71 eV and 285.91 eV); note the difference between lead (IV) and lead (II) carbonates.

The remaining C 1s lines are attributed as follows: (i)

hydrocarbons (**C**-C bonds): the '284.6 eV' standard line, which is found at 285.42 eV for the 'fresh' sample, 284.53 eV for both the '1 week old' and the 'annealed' sample; (ii) **C**-OH bonds at 286.94 eV for the 'fresh' sample, 286.26 eV for the '1 week old' sample and 285.91 eV for the 'annealed' sample, and (iii) O-**C**=O configurations for the line at 289.09 eV for the 'fresh' sample and 288.19 eV for the '1 week old' sample[28]. For a (Ti + Zr) unit, (contaminants) ≈ 3.92 (**C**-C) + 0.68 (**C**-OH) + 0.10 (O-**C**=O) for the 'fresh' sample, and ≈ 3.83 (**C**-C) + 0.82 (**C**-OH) + 0.51 (O-**C**=O) for the '1 week old' sample.
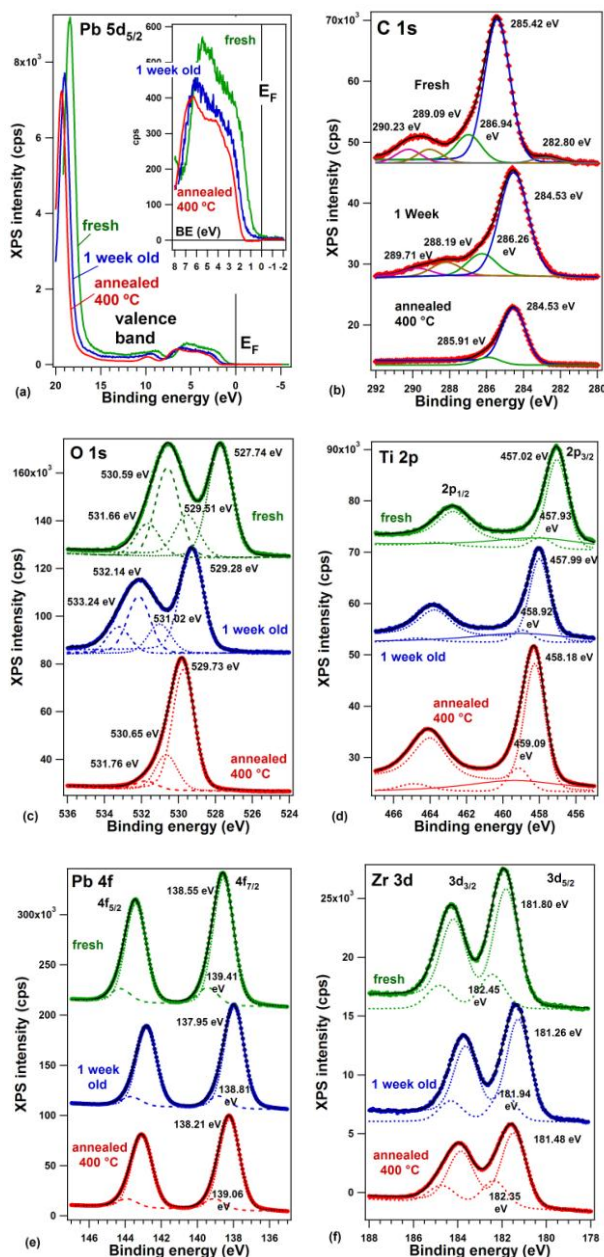
Fig. 2. XPS data for the three samples: (a) valence band spectra, with a zoom of the region near the Fermi level inserted; note the rigid shift of the Pb 5d3/2 level with the valence band onset; (b) C 1s electron distribution curves (EDCs); (c) O 1s EDCs; (d) Ti 2p EDCs; (e) Pb 4f EDCs; (f) Zr 3d EDCs.

The 'annealed' sample presents just 1.23 (**C**-C) in addition to the carbonate line. The remaining oxygen lines at 530.59 for the 'fresh' sample and at 532.14 eV for the '1 week old' sample represent adsorbed hydroxyl radicals[28,29]. Note also the presence of a small C 1s component at 282.80 eV for the 'fresh' sample.

Chemical shifts and electron attenuation effects

One observes from this analysis that all C 1s features from contaminants are located at about 0.9 ± 0.1 eV higher BE in the 'fresh' sample with respect to the '1 week old' sample. At the same time, the corresponding O 1s and Ti 2p levels from the substrate are located at 1.54 and 0.97 eV *lower* BE, respectively. The Zr 3d and Pb 4f levels are located at about 0.6 eV *higher* BE. Re-adjusting the binding energy scale by setting the C 1s maximum to its 'standard' value of adventitious carbon component (284.6 eV) doesn't solve the problem, since the Ti 2p and O 1s would shift at an unreasonable low BE. The key for solving this puzzle is to take into account the higher amount of molecules containing carbon bound to oxygen in the case of the '1 week old' sample, together with the known stronger bonding on $P^{(+)}$ areas[4-8]. Therefore, a mechanism such as the one represented in the Figure 3(a-c) may be invoked. Adsorption of contaminants takes place in a first instance onto $P^{(+)}$ areas, damping the corresponding XPS lines of the substrate, owing to inelastic mean free path effects. Hence, the substrate components (especially the Ti 2p and O 1s) which dominate the spectrum are those belonging to $P^{(-)}$ areas, shifted towards lower binding energies, according to the mechanism outlined in Figure 1. At the same time, the C 1s components from $P^{(+)}$ areas are shifted towards higher binding energies because of the surface band bending of these areas (Fig. 1).
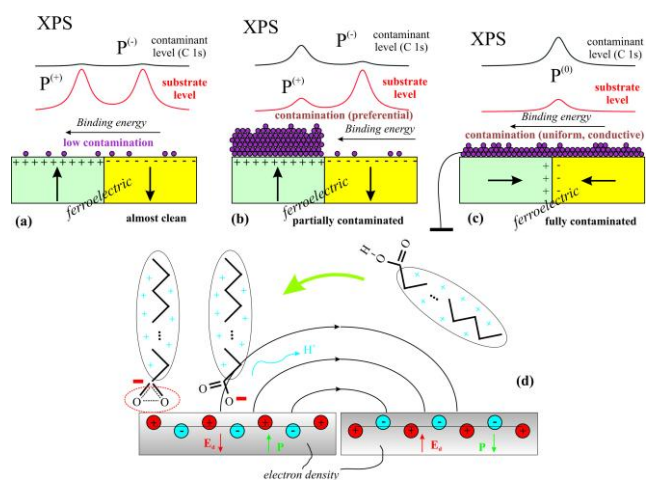
Fig. 3. (a) A surface with low contamination, with different signatures of outwards/inwards polarized areas; (b), the outwards polarized area starts to get contaminated; (c), the sample is fully contaminated; (d), mechanism proposed for preferential adsorption of fatty acids on areas with outwards polarization.

This implies also that the **C**-C component belong also to molecules which present a polar head attached to the surface; therefore, one may suppose that these molecules are on the form of alcohols R-OH, acids R-COOH, esters (etc.). The average size of the carbon chain R may be estimated for the 'fresh' sample from the '(contaminants)' approximate formula expressed in the previous paragraph as being about 3.92/(0.68 + 0.10) ≈ 5 C atoms. Taking into account attenuation effects of the **C**-O, O-**C**=O signals by the chains, the number of carbon atoms in chains

yields $(\lambda / d_0) \log(5\ d_0/\lambda + 1) \approx 4$, where $d_0 \approx 1.2 - 1.5$ Å is the average C-C distance[30] and $\lambda \approx 12$ Å is the C 1s inelastic mean free path[31]. Figure 3(d) presents such a mechanism. The negative charges of contaminant molecules, seen as electric dipoles, are located on the oxygen-containing heads, whereas the positive charges are delocalized on the whole alkyl chains. Attachment of the anionic heads to $P^{(+)}$ surface would be more favourable. In view of this mechanism, the low binding energy component of C 1s (282.80 eV) for the 'fresh' sample may be attributed to carbon adsorbed onto the $P^{(-)}$ areas, as represented also in Fig. 3(b).

The total intensity of the **C**-C component is about 20 % higher for the 'fresh' sample than for the '1 week old' sample. Therefore, the total amount of contaminants should be higher for the 'fresh' sample, despite the fact that these contaminants leave the $P^{(-)}$ areas uncovered. It seems that contaminants are 'stacked' together at the beginning on the $P^{(+)}$ areas, forming thicker layers: with progressive migration of contaminants on $P^{(-)}$ areas, combined with shortcuts realized by these molecular chains (or other effects combining charge transfer from adsorbates with loss of polarization, see below) the final result is the depolarization of the surface. Thus, the effective thickness of the contaminant layer diminishes when the full sample becomes contaminated. Eventually, the relatively large chain molecules stacking on the $P^{(+)}$ areas 'recumb' on the whole surface when the out-of-plane polarization domain structure is lost. Note that a similar loss of surface out-of-plane polarization was recently reported when Cu deposited on PZT(001) starts to form a continuous layer, connected to the ground of the system[18].
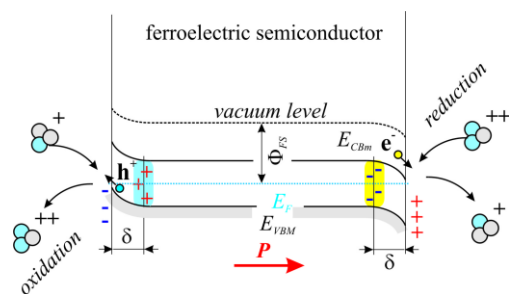
Fig. 4. Charge transport towards surfaces and possible catalytic activities of both surfaces (reduction for the outwards polarization, oxidation for the inwards polarization).

The actual results are at variance with X-ray photoemission electron microscopy (XPEEM) results[32], where a larger (by some 20-25 %) amount of carbon was detected on areas with inwards $P^{(-)}$ polarization. But in the above Reference the carbon state corresponding to the XPEEM maps was not specified (the C 1s spectrum is broad, and represented on a relative binding energy scale, centred on its maximum). It might happen that this carbon contains a non-neglectible amount of carbonates, therefore Ref. [32] just pointed out on the higher reactivity of $P^{(-)}$ surface to form carbonates than on the $P^{(+)}$ surface. In fact, it is clear that a negatively charged surface is more subject to be oxidized, and a positively charged surface offers is subject to reduction reactions. Therefore, at a negatively charged surface, contaminants will be decomposed (reduced) such as to produce anions (O^-, OH^-, $COOH^-$, CO_3^{2-}) which are expected to combine with initially partially reduced cations (Ti, Zr) $^{-\delta\ +4}$ or Pb$^{-\delta\ +4}$. The fact that $P^{(+)}$

surfaces offer potential for reduction reactions, and that $P^{(-)}$ surfaces offer potential for oxidation was already commented in the Introduction[11,12,33] and is schematized in Figure 4.

Thus, contaminants are expected to react with the $P^{(-)}$ areas, particularly carbon containing contaminants yield mostly carbonates, whereas they seem to be simply adsorbed on $P^{(+)}$ areas. The 'fresh' sample analyzed in this study is amongst the less contaminated ferroelectric thin film discussed in literature (and without any thermal treatment in ultrahigh vacuum). In this film, obviously the reactions yielding to carbonates were not accomplished and some parts of the $P^{(-)}$ areas remained free of contaminants, yielding the low binding energy components in the XPS spectra of the substrate.

The Pb 4f and Zr 3d spectra do not exhibit noticeable differences in binding energy. It was shown that upon copper deposition on $P^{(+)}$ oriented PZT, starting with a given Cu thickness, the surface band bending is lost, and this manifested in strong variation of O 1s and Ti 2p levels, weaker for Zr 3d and Pb 4f [18]. It seems that lead and zirconium are less sensitive to the polarization state of the surface. This has to be connected to the higher covalency character of Pb-O and Zr-O bonds, as compared with Ti-O bonds[18]. Therefore, any additional charge (induced by the depolarization field, or by adsorbates) seems to influence mostly Ti^{4+} and O^{2-} ions.

For the '1 week old' sample, both O 1s and Ti 2p main lines attributed to PZT are stabilized at energies intermediate between the value of the 'fresh' sample (which is now attributed to $P^{(-)}$ areas) and of the 'annealed' sample (which, in accordance with previous studies, is attributed to the $P^{(+)}$ state[18,20]). This mechanism is also sketched in the Figure 3(c): the contamination layer, owing to its large number of C atoms, will be conductive, promoting charge carriers from one polarized area to the neighboring one, such as to induce vanishing of the surface potential. Eventually, the polarization is switched in-plane near surface, and in-plane 180° ($\rightarrow\leftarrow$) domains may appear; but, in any case, the surface potential becomes constant, as for a sample with no out-of-plane polarization, and this is clearly seen in XPS. Note also that, if the fact that contamination induces a decrease in surface polarization is assumed, this may also explain the relatively low Schottky barriers obtained when metals are deposited onto PZT(001) by magnetron sputtering, i.e. not in ultrahigh vacuum[34] and the domination for some 'old' single crystal PZT(001) samples of areas with no out-of-plane surface polarization[15].

Piezoresponse force microscopy

Further evidence on the validity of this mechanism may be inferred from scanning probe microscopy images taken on a sample a few days old (Fig. 5). Topological defects affects less than 5 % of the surface, as can be seen from atomic force microscopy (AFM) images, with the exception of a few small (~ 50-100 nm) droplets (Fig. 5(a)). Phase PFM (Fig. 5(b)) was recorded after writing a well defined polarization pattern on the sample. It is found that the $P^{(-)}$ written areas (yellow square in Fig. 5(b)) subsist a few hours after writing, whereas asides of these area, where $P^{(+)}$ should have been present, the sample is in a higher amount in an unpolarized state. The complete process occurring when polarization is written on a contaminated sample may be that the contaminants are pushed away from the $P^{(-)}$ areas

towards the P$^{(+)}$ areas, a process which is in line with the one depicted in Fig. 3(d). PFM scans on freshly prepared samples (Fig. 5 of Ref. [15]) presented well defined P$^{(+)}$ and P$^{(-)}$ areas in comparable amount.
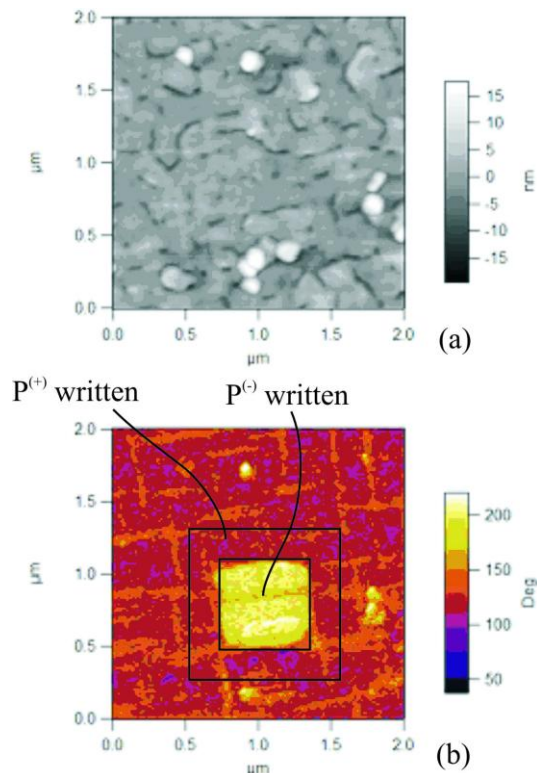
Fig. 5. Scanning probe microscopy analysis of a PZT sample a few days after its preparation: (a) topography (AFM) images; (b) phase PFM images taken on the same area, after PFM writing of polarization according to the drawn areas.

This implies that an interplay should exist between adsorption of contaminants and surface polarization states or, more specifically, between charge transfer induced by contaminants and the absolute value of the polarization. In a first approximation, the local polarization P may be connected to the charge density (assume that it is constituted by electrons of density n, for simplicity) by a simple law such as:

$$P = P_{max.} - p_0 \cdot n$$

where p_0 has the dimensions of a dipole moment and should be on the order of the dipole moment corresponding to an elementary cell of the ferroelectric. Such an equation may be justified by simple considerations. Consider the polarization oriented upwards. When some excess negative charge is provided to a ferroelectric elementary cell, part of this charge reduces the ionization state of the Ti^{4+} cation, and part of it is distributed on the upper and lower faces of the cell, by taking into account that the electrons already present on these faces are strongly hybrided O 2p and Pb 6p electrons. Thus, these faces can be seen as being occupied by delocalized electrons, similar to metals and additional electrons may be seen in a first approximation as being distributed uniformly on these faces. The new equilibrium condition may be calculated and connected to a reduced value of polarization, as function on the excess electron charge density,

and a linear dependence as the above may be obtained. More sophisticated Landau-Ginsburg-Devonshire theory gives similar results for the interplay between the remanent ferroelectric polarization and the charge density[35]. Note also that surface atomic displacements on ferroelectric BaTiO$_3$ were found by X-ray photoelectron diffraction considerably lower than that expected from the bulk polarization[36], which might be connected to both the presence of some contaminants on the sample surface, or to the charge accumulation near this free surface, according to Figs. 1 and 4.

Thus, there are chances that the polarization switching implied by the transition from Fig. 3(a) to Fig. 3(b) could eventually not (or not only) be due to an electrical shunt realized by the contaminants between areas with opposed polarization, but just to the progressive loss of surface ferroelectric polarization on contaminated areas, which induces the loss of preferential adsorption and the 'sloop' of contaminant molecules on adjacent areas. This problem is actually under investigation by spectro-microscopy techniques.

Conclusions

This work presented the analysis of surface core level shifts from PZT samples with different contamination levels. It was shown that the spectra of the freshly prepared samples can be explained only if one supposes that the contaminant molecules are polar and are attached in a large majority to areas of the sample presenting outwards polarization P$^{(+)}$. These molecules are (stacks of) chains containing an anionic head, with length (4-5 C atoms), sufficient to attenuate the substrate components from these areas. Only the areas of the sample presenting inwards polarization will manifest in the XPS spectra from the substrate. As soon as the sample gets more contaminated, two mechanisms are suggested: (i) Polar molecules start to be attached also to the areas with inwards polarization and, when the contamination layer becomes continuous, the induced band bending is compensated by the shortcut realized by the contaminants, which in this case start to lie down, parallel to the surface. (ii) The high amount of charge transferred from contaminants on P$^{(+)}$ areas induces progressively a loss of the surface polarization, implying the 'sloop' of contaminant molecules onto neighbouring areas of P$^{(-)}$ contamination. These two mechanisms may, of course, coexist.

O 1s and Ti 2p spectra are found to be much more sensitive to the charge state of the surface than Pb 4f and Zr 3d. This has to be connected to the ionic character of Ti-O bonds: eventual additional negative charge will partly reduce Ti^{4+} cations, and eventual additional positive charge will partly be localized on O^{2-} orbitals which form bonds with Ti^{4+}.

Sample surfaces thermally treated in ultrahigh vacuum may be simulated by a superposition of areas with outwards polarization P$^{(+)}$ and with no out-of-plane polarization P$^{(0)}$. Therefore, contaminants are easily removed from areas with outwards polarization. Such 'easy come easy go' behaviour of contaminants onto areas with well defined outwards polarization could be eventually exploited as an useful versatility in various catalytic processes.

Notes and references

a National Institute of Materials Physics, Atomistilor 105b, 077125 Măgurele-Ilfov, Romania. Fax: 40 21369 0177; Tel: 40 72429 1045; E-mail: laura.stoflea@infim.ro, nicoleta.apostol@infim.ro, lucian.trupina@infim.ro, *teodorescu@infim.ro

1   J.F. Scott, *Ferroelectric Memories*, Springer, Berlin, 2000.

2   K. Rabe, C.H. Ahn and J.M. Triscone, *Physics of ferroelectrics: a modern perspective*, Topics in Applied Physics 2007, **105**, 1-30.

3   M. Ciobanu, B. Cojocaru, C. Teodorescu, F. Vasiliu, S.M. Coman, W. Leitner, and V.I. Parvulescu, J. Catal. 2012, **296**, 43-54.

4   Y. Yun, L. Kampschulte, M. Li, D. Liao, and E.I. Altman, J. Phys. Chem. C 2007, **111**, 13951-13956.

5   Y. Yun and E.I. Altman, J. Am. Chem. Soc. 2007, **129**, 15684-15689.

6   M.H. Zhao, D.A. Bonnell, and J.M. Vohs, Surf. Sci. 2009, **603**, 284-290.

7   J. Garra, J.M. Vohs and D.A. Bonnell, Surf. Sci. 2009, **603**, 1106-1114.

8   M.J. Highland, T. T. Fister, D.D. Fong, P.H. Fuoss, C. Thompson, J.A. Eastman, S.K. Streiffer, and G.B. Stephenson, Phys. Rev. Lett. 2011, **107**, 187602.

9   J.L. Wang, F. Gaillard, A. Pancotti, B. Gautier, G. Niu, B. Vilquin, V. Pillard, G.L.M.P. Rodrigues, and N. Barrett, J. Phys. Chem. C 2012, **116**, 21802-21809.

10 K. Garrity, A.M. Kolpak, S. Ismail-Beigi, and E.I. Altman, Adv. Mater. 2010, **22**, 2969-2973.

11 Y. Cui, J. Briscoe and S. Dunn, Chem. Mater. 2013, **25**, 4215-4223.

12 D.B. Li, M.H. Zhao, J. Garra, A.M. Kolpak, A.M. Rappe, D.A. Bonnell, and J.M. Vohs, Nature Mater. 2008, **7**, 473-477.

13 S.J.A. Moniz, R. Quesada-Cabrera, C.S. Blackman, J.W. Tang, P. Southern, P.M. Weaver, and C.J. Carmalt, J. Mater. Chem. A 2014, **2**, 2922-2927.

14 F. Chen and A. Klein, Phys. Rev. B 2012, **86**, 094105.

15 N.G. Apostol, L.E. Stoflea, G.A. Lungu, C. Chirila, L. Trupina, R.F. Negrea, C. Ghica, L. Pintilie, and C.M. Teodorescu, Appl. Surf. Sci. 2013, **273**, 415-425.

16 N.G. Apostol, L.E. Stoflea, G.A. Lungu, L.C. Tanase, C. Chirila, L. Frunza, L. Pintilie, and C.M. Teodorescu, Thin Solid Films 2013, **545**, 13-21.

17 N.G. Apostol, L.E. Stoflea, G.A. Lungu, C.A. Tache, L. Pintilie, and C.M. Teodorescu, Mater. Sci. Eng. B 2013, **178**, 1317-1322.

18 L.E. Stoflea, N.G. Apostol, C. Chirila, L. Trupina, R. Negrea, L. Pintilie, and C.M. Teodorescu, J. Mater. Sci. 2014, **49**, 3337-3351.

19 L. Pintilie and M. Alexe, J. Appl. Phys. 2005, **98**, 124103.

20 I. Vrejoiu, M. Alexe, D. Hesse, and U. Gösele, Adv. Funct. Mater. 2008, **18**, 3892-3906.

21 D. Marton, K.J. Boyd, A.H. Al-Bayati, S.S. Todorov, and J. Rabalais, Phys. Rev. Lett. 1994, **73**, 118-121.

22 B.D. Ratner and D.G. Castner, in *Surface Analysis - The Principal Techniques*, 2nd Ed., J.C. Vickerman and I.S. Gilmore (Eds.), Wiley, New York, 2009, p. 47.

23 N.G. Gheorghe, G.A. Lungu, M.A. Husanu, R.M. Costescu, D. Macovei, and C.M. Teodorescu, Appl. Surf. Sci. 2013, **267**, 106-111.

24 R.M. Costescu, N.G. Gheorghe, M.A. Husanu, G.A. Lungu, D. Macovei, I. Pintilie, D.G. Popescu, and C.M. Teodorescu, J. Mater. Sci. 2012, **47**, 7225-7234.

25 F. Chen, R. Schafranek, W.B. Wu, and A. Klein, J. Phys. D: Appl. Phys. 2011, **44**, 255301.

26 C.M. Teodorescu, J.M. Esteva, R.C. Karnatak, and A. El Afif, Nucl. Instrum. Meth. Phys. Res. A 1994, **345**, 141-147.

27 D. Luca, C.M. Teodorescu, R. Apetrei, D. Macovei, and D. Mardare, Thin Solid Films 2007, **515**, 8605-8610.

28 M. Iliut, C. Leordean, V. Canpean, C.M. Teodorescu, and S. Astilean, J. Mater. Chem. C 2013. **1,** 4094-4104.

29 Y. Tanaka, H. Saito, Y. Tsutsumi, H. Doi, H. Imai, and T. Hanawa, Mater. Trans. 2008, **49**, 805-811.

30 *CRC Handbook of Chemistry and Physics*, 75th Edition, D.R. Lide (Ed.-in-Cief), CRC Press, Boca Raton, 1994, p. **9**-1.

31 S. Hüfner, *Photoelectron Spectroscopy: Principles and Applications*, 3rd Edition, Springer, Berlin, 2003, p. 9.

32 I. Krug, N. Barrett, A. Petraru, A. Locatelli, T.O. Mentes, M.A. Niño, K. Rahmanizadeh, G. Bihlmayer, and C. M. Schneider, Appl. Phys. Lett. 2010, **97**, 222903.

33 R. Ferris, B. Yellen and S. Zauscher, Small 2012, **8**, 28-35.

34 I. Pintilie, C.M. Teodorescu, C. Ghica, C. Chirila, A.G. Boni, L. Hrib, I. Pasuk, R. Negrea, N.G. Apostol, and L. Pintilie, ACS Adv. Mater. Interf. 2014, **6**, 2929-2939.

35 P. Zubko, D.J. Jung, and J.F. Scott, J. Appl. Phys. 2006. **100**, 114112.

36 A. Pancotti, J. Wang, P. Chen, L. Tortech, C.M. Teodorescu, E. Frantzeskakis, N. Barrett, Phys. Rev. B 2013, **87**, 184116.